Aquatic Geochemistry (2018) 24:209–229
https://doi.org/10.1007/s10498-018-9340-3

Salt Crystallization Sequences of Nonmarine Brine and Their Application for the Formation of Potassium Deposits

Chuanyong Ye[1] · Jianye Mao[2] · Yaqiong Ren[1] · Yingping Li[3] · Yongjie Lin[4] · Ian M. Power[5] · Yangbing Luo[1]

Received: 13 March 2018 / Accepted: 27 June 2018 / Published online: 5 July 2018

Abstract
The salt assemblages precipitated during evaporation of concentrated brine collected from Gasikule Salt Lake (GSL) were studied to better understand the formation of potassium deposits in the Qaidam Basin. The study included isothermal evaporation at 25 °C in the laboratory and solar evaporation in the ponds at GSL field. Brines increased in density and became moderately acidic (pH ≈ 5.30) while major ion geochemistry and precipitate mineralogy all showed broad agreement between both systems. Four salt assemblages were identified in the isothermal evaporation experiment: halite → halite + hexahydrite → halite + bischofite + carnallite → bischofite. Alternately, three salt assemblages were recognized in the solar evaporation: halite → halite + epsomite + carnallite → halite + carnallite + bischofite. The key difference in salt assemblages between the two systems is attributed to differences in relative humidity and temperature conditions. Although the GSL has deep spring inflow recharge, the high abundance of $MgSO_4$ salts demonstrates that the salt assemblages are similar to normal seawater evaporation. Thus, different proportions of deep spring inflow and river water could form both $MgSO_4$-deficient potassium evaporite and normal seawater potassium evaporites. Therefore, nonmarine water may form diverse potassium evaporite deposits in continental basins when the geological structure as well as hydrogeological and climatic conditions is appropriate.

Keywords Isothermal evaporation · Solar evaporation · Nonmarine brine · Potassium deposits · Qaidam Basin

1 Introduction

Ancient potassium evaporite deposits fall into two groups: (1) an $MgSO_4$-bearing group with mineral assemblages predicted to form from evaporative concentration of seawater with the composition of today's oceans and (2) an $MgSO_4$-poor group with mineral assemblages that cannot be derived from the evaporation of modern seawater. The most abundant

✉ Yangbing Luo
luoyangbing0319@126.com

Extended author information available on the last page of the article

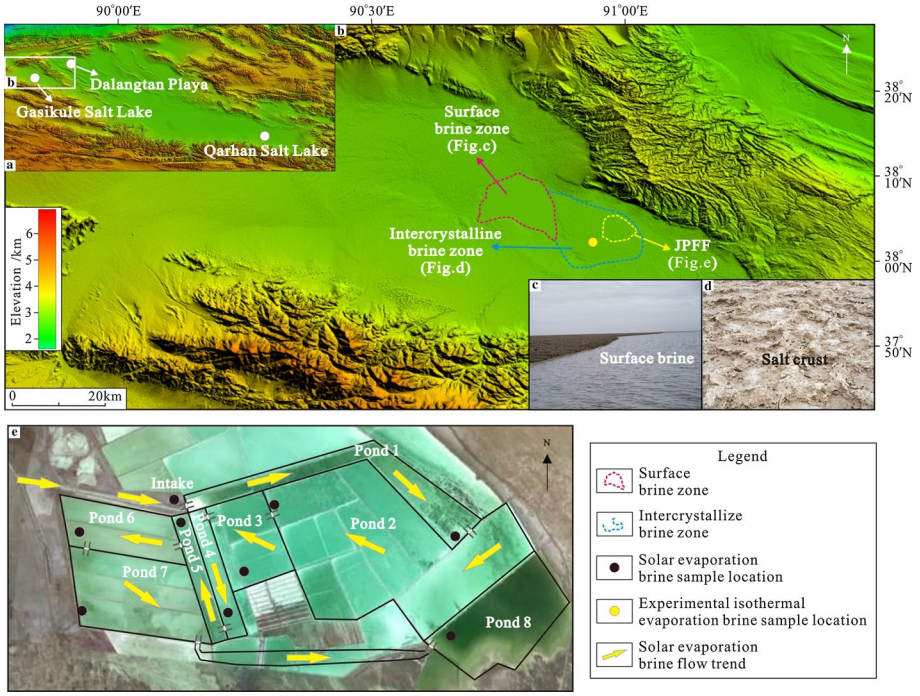

Fig. 1 Map of the study area: **a** locations of GSL, Dalangtan Playa and Qarhan Salt Lake at the Qaidam Basin, **b** locations of surface brine zone, intercrystalline brine zone and Jingxin Potash Fertilizer Factory (JPFF) at the GSL, **c**, **d** surface morphology of surface brine zone and intercrystalline brine zone and **e** concentration ponds at JPFF site

potassium deposits are composed of the latter group, and their origin remains unresolved (Hardie 1990).

Several hypotheses have been proposed to explain the formation of potassium evaporite deposits such as parent waters (seawater versus nonmarine inflow), depositional environments (deep versus shallow waters) and timing of formation type (primary precipitates versus diagenetic alteration products), yet there remain uncertainties. One confounding factor is that there are few detailed studies of any modern potash-bearing basins. The Qaidam Basin, in the northernmost part of the Qinghai–Tibetan Plateau (QTP), is one of the few locations in the world where significant quantities of potash salts are forming today (Casas et al. 1992; Zhang 1987). Consequently, the Qaidam Basin is an important natural setting to study the origin of potash salts including the brines from which these salts form. It is important to note that this is a large, nonmarine basin which contains extensive salt deposits. The processes that lead to potash salt deposition in the Qaidam Basin have application for understanding ancient potash deposits in both marine and nonmarine settings (Spencer et al. 1990), specifically the Dalangtan Playa and Qarhan Salt Lake that are located at the northwestern and middle of the Qaidam Basin, respectively (Fig. 1a).

Evaporite minerals identified in Dalangtan Playa include halite, carnallite, gypsum, anhydrite, mirabilite, glauberite, meridianiite, epsomite, hexahydrite, pentahydrite, starkeyite, sanderite and kieserite (Kong et al. 2014; Wang et al. 2016). Mineral formulas are given in Table 1. Clearly, Dalangtan Playa contains large quantities of $MgSO_4$ salts, which

Table 1 Mineral formulas of solid phases in this study

Name	Chemical composition
Halite	$NaCl$
Carnallite	$KCl{\cdot}MgCl_2{\cdot}6H_2O$
Gypsum	$CaSO_4{\cdot}2H_2O$
Anhydrite	$CaSO_4$
Mirabilite	$Na_2SO_4{\cdot}10H_2O$
Glauberite	$Na_2SO_4{\cdot}CaSO_4$
Meridianiite	$MgSO_4{\cdot}11H_2O$
Epsomite	$MgSO_4{\cdot}7H_2O$
Hexahydrite	$MgSO_4{\cdot}6H_2O$
Pentahydrite	$MgSO_4{\cdot}5H_2O$
Starkeyite	$MgSO_4{\cdot}4H_2O$
Sanderite	$MgSO_4{\cdot}2H_2O$
Kieserite	$MgSO_4{\cdot}1H_2O$
Calcite	$CaCO_3$
Dolomite	$CaMg(CO_3)_2$
Aragonite	$CaCO_3$
Magnesite	$MgCO_3$
Sylvite	KCl
Bischofite	$MgCl_2{\cdot}6H_2O$
Tachyhydrite	$CaMg_2Cl_6{\cdot}12H_2O$
Polyhalite	$K_2SO_4{\cdot}MgSO_4{\cdot}2CaSO_4{\cdot}2H_2O$
Thenardite	Na_2SO_4
Glaserite	$3K_2SO_4{\cdot}Na_2SO_4$
Schoenite	$K_2SO_4{\cdot}MgSO_4{\cdot}6H_2O$
Astrakanite	$Na_2SO_4{\cdot}MgSO_4{\cdot}4H_2O$

is consistent with the evaporite deposits in the Western Europe magnesite Mesozoic salt basin represented by the German Stassfurt potassium deposit. Importantly, the mineral sequence is very similar to the normal seawater evaporative sequence.

The Qarhan Salt Lake, the largest salt lake in the Qaidam Basin and one of the most famous inland salt lakes in the world, contains the largest potassium deposit in China (Fan et al. 2015; Wang et al. 2014b; Warren 2016; Zheng 2011). The assemblage of evaporite minerals in the lake is relatively simple and does not contain $MgSO_4$ salts. The deposit comprises mainly calcite (a small amount of dolomite, aragonite and magnesite), gypsum (anhydrite), halite and carnallite (little sylvite) (Chen and Bowler 1986; Zhang et al. 1993). The mineral assemblages of Qarhan Salt Lake are similar to early Cretaceous evaporite deposits in the Congo rift basin (Pedley et al. 2016; Timofeeff et al. 2006; Zhang et al. 2017), the Late Cretaceous evaporites in the Khorat Plateau (Eastoe et al. 2007; Timofeeff et al. 2006; Wang et al. 2014a; Zhang et al. 2015, 2016), the Permian Salado Formation, New Mexico (Casas et al. 1992), and the middle Devonian Prairie Formation, Saskatchewan, Canada (Jensen et al. 2006). They have been called $MgSO_4$-deficient evaporites because they lack $MgSO_4$ salts that are different from the characteristic of a normal seawater evaporation sequence (Lowenstein et al. 1989). The Qarhan Salt Lake potassium deposit was studied by Lowenstein and Risacher (2008, Lowenstein et al. (1989), Casas

et al. (1992) and Zhang et al. (1993) who proposed that the brines were derived from meteoric river inflow mixed with small amounts of CaCl spring inflow similar in composition to many saline formation waters and hydrothermal brines. Evaporation of CaCl spring inflow yields a predicted mineral sequence including carnallite, bischofite and tachyhydrite that is identical to several anomalous marine evaporites. Deep CaCl spring inflow is a key factor in the formation of $MgSO_4$-deficient potassium salt in the Qarhan Salt Lake. Moreover, a mixture of river water to deep CaCl spring water of less than 40:1 can produce the current brine.

The mineral assemblages in the Qarhan Salt Lake do not contain $MgSO_4$ salts, whereas the Dalangtan Playa contains abundant $MgSO_4$ salts. These playas are all located in the Qaidam Basin and belong to a nonmarine metallogenic environment, yet the mineral assemblages are highly variable. Thus, nonmarine brines in inland continental basins may form either the so-called $MgSO_4$-deficient potassium evaporation salts or the normal seawater mineral assemblages. When considering previous research, there are two questions that arise: Is deep CaCl spring inflow a necessary condition for the formation of $MgSO_4$-deficient potassium deposits? And, if there is deep CaCl spring inflow supply, does the ratio between river water and deep CaCl spring inflow need to be 40:1? To answer these questions, we examined CaCl spring inflow into salt lakes in the Qaidam Basin and determined the mineral assemblages during brine evaporation.

A preliminary study showed that the GSL, located at the western of the Qaidam Basin, is partly supplied by deep CaCl springs, and its brine has a high concentration of potassium (average = 4.43 mg/L) (Ye et al. 2015). Building on this study, we carried out an isothermal evaporation experiment to determine the salt precipitation sequences with a particular focus on $MgSO_4$ salts to answer the two aforementioned research questions. Given that there are challenges when comparing laboratory results to natural processes, we also studied the mineral assemblages during natural evaporation in solar ponds. Currently, a company uses the brine as raw material to produce potash fertilizer by evaporation in these ponds.

In this study, we have determined the mineral assemblages of isothermal evaporation in the laboratory and solar evaporation in the field of the GSL at the western of the Qaidam Basin. The goals of this study were: (1) to determine the crystallization boundaries between the various dissolved mineral salts in the brine of GSL, (2) distinguish and explain the differences in the mineral composition between isothermal evaporation and solar evaporation and (3) provide the mineral clues for the origin of nonmarine potassium deposits in the Qinghai-Tibet Plateau and ancient potassium evaporites.

2 Methods

2.1 Site Description

The Qaidam Basin is a closed, nonmarine basin with an area of 120,000 km^2 (Fig. 1a). The center of the present basin, 2800 m above sea level, contains large dry areas underlain by salt and many shallow (< 1 m deep) saline lakes that precipitate salts, including potash minerals (Chen and Bowler 1986).

GSL is situated at the western tip of the Qaidam Basin and is the modern center of the Gasikule depression (Wang et al. 2013). The region has an arid continental climate and receives only 55 mm of rainfall on average while evaporation rates are approximately

2857 mm yr^{-1}. Mean annual air temperature is 3 °C and may exceed 30 °C in summer (July) and reach lows below −20 °C in the winter (January). Winds can reach maximums of 40 m s^{-1} and primarily come from the NW and NNW. Because of the dry climate and lack of outlets, lake waters gradually evaporate driving an increase in salinity that leads to salt formation. The oldest salt deposit was dated at 608 ± 38 ka (Wang et al. 2013). The lake is divided into two zones: a surface brine zone to the west and an intercrystalline brine zone to the east (Fig. 1b). The surface brine zone maintains water throughout the year and with a maximum depth exceeding 1 m in spring (Fig. 1c). In contrast, the intercrystalline brine zone consists of a surface salt crust with well-developed polygonal honeycomb-shaped structures surrounded by a dry saline mudflat and floored by layered halite with permanent groundwater brine located at a depth of 0–1.2 m (Fig. 1d). The surface salt crust is commonly rugged and consists predominantly of a mixture of fine-grained halite and mud. Vadose diagenetic features, such as dissolution pipes and cavities and pendant cements, occur where the surface salt crust lies above the water table (Ye et al. 2015).

To developed brine resources, the local government built a potash fertilizer factory, Jingxin Potash Fertilizer Factory (JPFF), in the northeastern area of the intercrystalline brine zone (Fig. 1b). The JPFF is 8 km from the surface brine zone and has eight solar ponds with an annual capacity of 100,000 tonnes of potassium sulfate. The salt extraction process at JPFF is based on brine concentration technology via evaporation–precipitation cycles using solar energy. Intercrystalline brine is pumped into storage auxiliary ponds (ponds 1, 2 and 3) where halite (NaCl) is precipitated (Fig. 1e). The brine is highly saline, and the main compositions in ponds 1, 2 and 3 are Na, K, Mg, Cl and SO_4. After halite precipitation, the residual brine (the bittern) is enriched in potassium–magnesium salts (K–Mg salts). The residual bittern is pumped from the pond 3 as the raw brine feed for pond 4. Through a brine mixing process, this highly saline brine is supersaturated with respect to epsomite and carnallite in ponds 4, 5, 6 and 7. After epsomite and carnallite precipitation, the residual brine is enriched in magnesium salts (Mg salts) and is then fed into pond 8. Brine in pond 8 was supersaturated with respect to carnallite and bischofite.

2.2 Fieldwork

Brine and evaporite deposits (solid samples) at each JPFF pond were collected in May 2010 (Fig. 2a). Intercrystalline brine used for the isothermal evaporation was also collected from the transportation channel (Fig. 2b). At the time of sampling, the weather at the field site was dry and hot with no rainfall occurring. The average temperature at the site was 10 °C with an average relative humidity (RH) of 37% (data from JPFF meteorological station).

Measurements of pH and temperature of brines were taken in the field using a HACH digital and portable multi-parameter meter. Densities were measured using a hydrometer with data being corrected for temperature. All samples were filtered through 0.45-μm glass fiber membrane filters. Samples for cation analysis were acidified with HNO_3 to pH < 2 and stored in 50- or 100-mL polyethylene bottles. The brine samples were diluted twofold with distilled water to avoid any further precipitation.

In addition to the brines, salt samples from each pond were collected in plastic bags and tightly sealed in the field. The salt samples were kept isolated from the atmosphere prior to analysis.

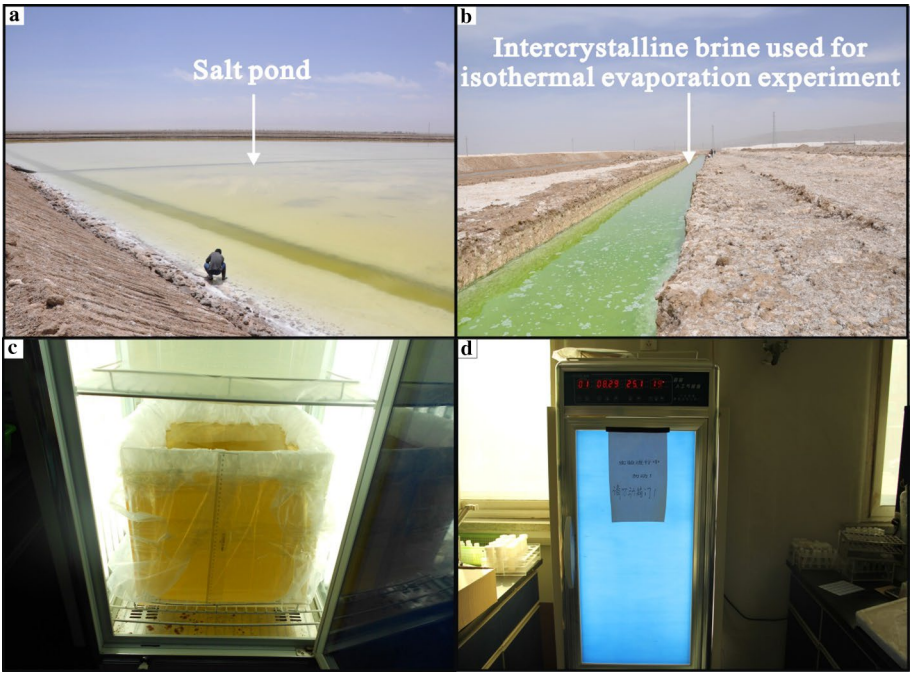

Fig. 2 Field sampling of a solar evaporation pond (**a**) and intercrystalline brine (**b**), as well as the crystallizer (**c**) and thermotank (**d**) used in the isothermal evaporation experiment

2.3 Isothermal Experimental Methods

An isothermal evaporation experiment was conducted at the Beijing Research Institute of Uranium Geology, Beijing, China. Intercrystalline brine (60 L) with a starting density of 1.18 g/mL was dispensed into a $40 \times 40 \times 40$ cm organic glass crystallizer. The crystallizer was placed in a thermotank where evaporation commenced (Fig. 2c, d). The brine was kept at a constant temperature of 25 ± 0.1 °C and relative humidity of 45%. An incandescent lamp simulated sunlight for 12 h per day and ensured that the solution temperature was maintained at 25 ± 0.1 °C.

The brine behavior and characteristics were regularly documented during the experiment that lasted for 356 days. As expected, the brine volume decreased during the experiment. Newly precipitated salts were analyzed and the pH and density of the brine were measured each day. Brines and precipitates were collected regularly to monitor water chemistry and precipitate mineralogy (Table 2). The crystal morphologies of precipitated salts were observed by scanning electron microscope (Hitachi TM-1000, Japan). A Büchner funnel was used to remove the salt from brine when the new salt assemblages appeared.

For chemical analyses, brines were diluted twofold with distilled water to avoid further precipitation. Simultaneously, small amounts of precipitated salt were gently filtered and stored in plastic bags for mineralogical analysis.

Table 2 Description of the brines and salts in the isothermal evaporation

Evaporation time (days)	Brine		Salts	
	Sample	Description	Sample	Description
0	GSHZF12-1	Light green		
14	GSHZF12-2	Light green		
35	GSHZF12-3	Light green	GSHZFG12-1	White, cubic
44	GSHZF12-4	Light green	GSHZFG12-2	White, flakey and cubic
69	GSHZF12-5	Light green	GSHZFG12-3	White, cubic
107	GSHZF12-6	Light green	GSHZFG12-4	White, cubic with fine-grained cements
181	GSHZF12-7	Light green	GSHZFG12-5	White, cubic and octahedral
225	GSHZF12-8	Light green	GSHZFG12-6	White, cubic
268	GSHZF12-9	Light green	GSHZFG12-7	White, cubic
315	GSHZF12-10	Light green, microviscosity	GSHZFG12-8	White, fine-grained
357	GSHZF12-11	Light green, high viscosity	GSHZFG12-9	White, columnar

2.4 Analytical Techniques

Brines were analyzed for major cations (K^+, Na^+, Ca^{2+}, Mg^{2+}) and anions (Cl^-, SO_4^{2-}, and HCO_3^-) at the Analytical Laboratory of Beijing Research Institute of Uranium Geology by ion chromatography (DIONEX, DX-500) (Ye et al. 2015).

Mineral identifications of evaporites were determined by XRD powder diffraction using a PANalytical diffractometer, model X'PERT PRO MPD (PW 3040/60), with a goniometer equipped with a copper anode and Cu-Ka (40 kV, 40 mA). The instrument is electronically controlled and operates with expert data collector and X'Pert HighScore Plus identification software that runs with the International Centre for Diffraction Database (Tait et al. 2017). During the XRD data analysis, the lattice spacing d (Å) values and relative intensities (I/I_o) of the reflection peaks as a function of 2θ have been compared with the Joint Committee on Powder Diffraction Standards (JCPDS 1980).

3 Results and Discussion

Major ion geochemistry and densities of brines from the isothermal evaporation and solar evaporation are provided in Table 3.

3.1 Brine pH Changes

At the same densities, the pH of the brines in the solar evaporation ponds was lower than in the isothermal evaporation experiment. This discrepancy is attributed to the ponds being closer to equilibrium with atmospheric CO_2. Brines in both systems exhibited an acidification trend with increasing density caused by evaporation, which is similar to the Zhabei Salt Lake, Tibet (Gao et al. 2012; Zheng and Liu 2009) (Fig. 3). With the gradual decrease in massive neutral compositions as sodium chloride, sodium sulfate and water,

Table 3 Major ion compositions (g/L) of isothermal evaporation brines and solar evaporation brines measured at different pH and densities

Sample name	Cl^-	SO_4^{2-}	HCO_3^-	Na^+	K^+	Mg^{2+}	Ca^{2+}	pH	Density (g/mL)	*T* (°C)
Isothermal evaporation at 25 ± 0.1 °C										
GSHZF12-1	160.68	32.26	0.26	78.80	2.95	19.35	1.80	7.34	1.18	25 ± 0.1
GSHZF12-2	182.03	35.70	0.02	89.20	2.75	20.80	1.05	7.37	1.19	25 ± 0.1
GSHZF12-3	181.78	48.90	0.37	86.30	3.00	25.05	0.85	7.21	1.24	25 ± 0.1
GSHZF12-4	192.47	50.67	0.51	81.75	3.30	27.30	0.75	7.27	1.25	25 ± 0.1
GSHZF12-5	198.02	101.30	0.72	55.60	6.60	55.05	0.85	6.96	1.27	25 ± 0.1
GSHZF12-6	206.30	76.91	2.79	23.05	10.65	68.15	1.45	6.78	1.29	25 ± 0.1
GSHZF12-7	232.14	41.72	2.69	5.10	7.30	91.95	0.00	5.98	1.32	25 ± 0.1
GSHZF12-8	289.92	37.87	1.89	1.80	1.05	114.40	0.00	5.64	1.33	25 ± 0.1
GSHZF12-9	306.32	26.30	2.11	1.15	0.65	118.05	2.40	5.54	1.36	25 ± 0.1
GSHZF12-10	311.02	28.05	2.35	1.05	0.50	117.05	2.45	5.52	1.35	25 ± 0.1
GSHZF12-11	296.76	25.40	3.20	1.10	0.55	111.60	2.25	5.40	1.35	25 ± 0.1
Solar evaporation at each pond of JPFF										
Intake	186.28	46.62	1.08	67.29	6.54	41.37	0.17	6.93	1.24	9.43
Pond 1	192.78	48.88	1.11	55.48	7.04	53.62	0.14	6.78	1.24	15.08
Pond 2	202.19	52.72	1.16	41.51	7.66	60.63	0.13	6.60	1.25	15.70
Pond 3	208.31	49.94	1.28	38.59	8.02	63.35	0.12	6.54	1.25	16.80
Pond 4	215.43	47.73	1.52	19.90	9.28	76.83	0.11	6.41	1.26	18.60
Pond 5	225.53	43.85	1.64	27.75	9.91	74.77	0.11	6.33	1.26	21.97
Pond 6	308.14	31.59	2.79	7.09	1.93	113.11	0.04	5.43	1.31	19.83
Pond 7	267.69	33.79	2.13	18.60	2.28	89.20	0.07	5.96	1.28	21.38
Pond 8	329.11	28.86	2.00	4.65	0.84	113.36	0.03	5.20	1.33	26.40

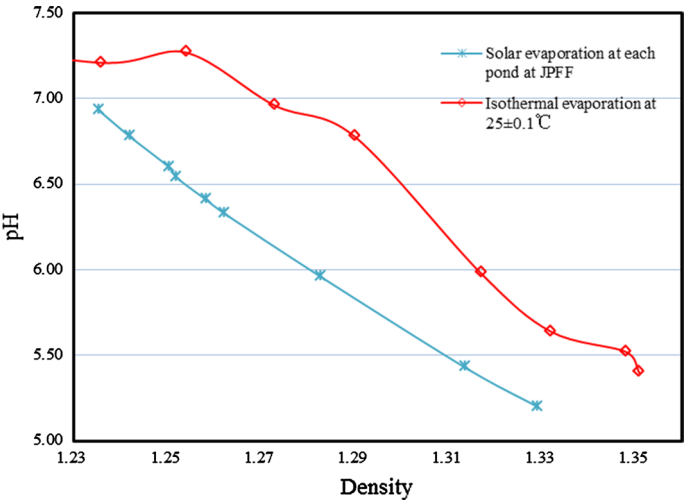

Fig. 3 Density versus pH of brines at the isothermal evaporation and solar evaporation

the proportion of strong acid–weak base salts becomes increasingly greater, and then the hydrolysis of these salts acidifies the brine systems. In other words, H^+ ions are being concentrated while the salts are not neutralizing the acidity.

In the isothermal evaporation experiment, the change in pH was small prior to the density reaching 1.25 g/mL, but the acidification tendency was significant after this point (Fig. 3). This was due to the low concentration of carbonate and bicarbonate that is in equilibrium with CO_2 in the air existing at brine during evaporation. At the beginning stage, it is very simple to increase the concentration of alkalinity; it will make the pH value slightly rise. However, this kind of fluctuation range is small and generally does not affect the general acidification trend.

3.2 Crystallization Paths

The Jänecke phase diagram is a useful tool for illustrating the crystallization paths during evaporation of brines with a five-component system (Na^+, K^+, Mg^{2+}‖Cl^-, SO_4^{2-}–H_2O) at different temperatures (Abdel Wahed et al. 2015; Eugster et al. 1980; Sun et al. 2002). Brines from the isothermal evaporation experiment and solar evaporation of GSL were mainly composed of K^+, Na^+, Mg^{2+}, Cl^- and SO_4^{2-} (Table 3). A temperature of 25 °C is suitable given that samples were collected during the summer during hot and dry conditions. Accordingly, the Jänecke phase diagram at 25 °C that includes Na^+, K^+, Mg^{2+}‖Cl^-, SO_4^{2-}–H_2O system is suitable for the present case.

In this diagram, the Jänecke coordinates (mole $\sum K_2 + Mg + SO_4 = 100$) for a considered solution are expressed in Eq. 1 (Eugster 1980):

$$K_2\% = n\left[K_2\right]/D * 100, Mg\% = n\left[Mg\right]/D * 100 \text{ and } SO_4\% = n\left[SO_4\right]/D * 100, \tag{1}$$

where n is the mole number and $D = n[K_2] + n[Mg] + n[SO_4]$.

In applying the Jänecke diagram, it is assumed that the solution is (1) halite saturated, meaning it will co-precipitate halite with the other salt phases separated during evaporation and (2) calcium and dissolved carbonate species are thought to be inconsequential constituents because their concentrations in the saturated solutions are low (Eugster 1980). However, Ca-bearing phases such as gypsum ($CaSO_4{\cdot}2H_2O$) or anhydrite ($CaSO_4$) may react with brines to produce glauberite ($Na_2SO_4{\cdot}CaSO_4$) and polyhalite ($K_2SO_4{\cdot}MgSO_4{\cdot}2CaSO_4{\cdot}2H_2O$), thus profoundly affecting the subsequent evolution of the evaporating brine (Eugster 1980). These types of reactions are not expected to occur in the isothermal evaporation experiment or solar evaporation ponds because the original brines were saturated with respect to $CaCO_3$ phases and aragonite was separated. Thus, the brines in GSL were initially free of Ca-bearing minerals.

Qinghai Lake is the largest inland continental lake in the Qaidam Basin of China. Sun et al. (2002) studied the chemical evolution of brines during evaporation. Similarly, this study seeks to compare the crystallization sequences predicted by the Jänecke phase diagram with the crystallization sequences determined for the isothermal evaporation experiment and solar evaporation ponds. The Jänecke coordinates of K_2, Mg and SO_4 of the brines were calculated from the data given in Table 3 and listed in Table 4. The initial brines deviate and lie on the crystallization path of Qinghai Lake water, respectively (Fig. 4). Both initial brines were more concentrated and at a more progressive evaporation stage in comparison with the Qinghai Lake water. The crystallization paths for the isothermal evaporation experiment and solar evaporation ponds were in good agreement with the

Table 4 Jänecke coordinates of K_2, Mg and SO_4 during the isothermal evaporation and solar evaporation

Sample name	K_2 %	Mg %	SO_4 %	Sample name	K_2 %	Mg %	SO_4 %
Isothermal evaporation				Solar evaporation			
GSHZF12-1	3.23	68.06	28.71	Intake	3.68	74.94	21.38
GSHZF12-2	2.79	67.77	29.44	Pond 1	3.21	78.64	18.15
GSHZF12-3	2.43	65.30	32.26	Pond 2	3.12	79.40	17.48
GSHZF12-4	2.49	66.34	31.16	Pond 3	3.18	80.72	16.10
GSHZF12-5	2.48	66.53	30.99	Pond 4	3.14	83.70	13.16
GSHZF12-6	3.64	74.95	21.41	Pond 5	3.46	84.06	12.48
GSHZF12-7	2.17	87.76	10.08	Pond 6	0.49	92.94	6.57
GSHZF12-8	0.26	92.03	7.71	Pond 7	0.40	90.88	8.71
GSHZF12-9	0.16	94.51	5.33	Pond 8	0.22	93.74	6.04
GSHZF12-10	0.13	94.16	5.71				
GSHZF12-11	0.14	94.42	5.44				

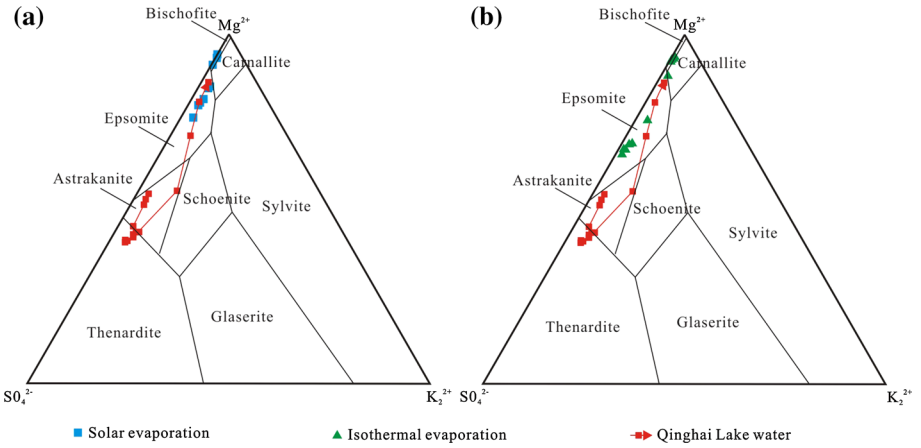

Fig. 4 Jänecke phase diagram (mole $\sum K_2 + Mg + SO_4 = 100$) at 25 °C showing **a** solar evaporation crystallization path and **b** isothermal evaporation crystallization path. The diagram and the Qinghai Lake water crystallization path are redrawn from Sun et al. (2002)

predicted crystallization paths of Qinghai Lake water (Fig. 4); however, the evaporation process stopped at bischofite phase in both cases. This difference in endpoint is possibly due to the extremely high salinities in our systems, which may result in the brines being hygroscopic and adsorbing humidity from the air rather than drying in the Qinghai Lake water evaporation experiment.

3.3 Variation of the Different Ions as a Function of Density

The crystallization sequences for the isothermal evaporation experiment and solar evaporation at the JPFF ponds were investigated by tracking ion concentrations and precipitate mineralogy along with density changes.

Major ion concentrations are represented as mol/1000 mol H_2O as recommended for the study of brine evolution during evaporation (McCaffrey et al. 1987). Accordingly, the numbers of moles of ions per 1000 mol H_2O as a function of density are calculated using Eq. 2 given by Zayani et al. (1999):

$$(C_i)_j = \frac{(c_i)_j 1000}{M_i (n_{H_2O})_j}, \tag{2}$$

where $(C_i)_j$ is the concentration of ion (i) in the sample (j), expressed in moles per 1000 mol of water, $(c_i)_j$ is the concentration in g L^{-1} of the ion (i) in the sample (j), M_i is the molar mass of the ion (i) and (nH_2O) is the number of moles of water in 1 L of the sample (j).

The evolution of major ions during progressive evaporation is based on the initial concentrations of these ions at the beginning of evaporation. In other words, it is based on the principle of "chemical divide." A chemical divide is a point in the brine evolution sequence when precipitation of a mineral depletes the water of certain cations or anions and further evaporation moves the solution along a distinct pathway. The basic idea of the chemical divide rule is that when a binary salt is precipitated, and the initial molar proportion of the two ions forming this salt is not equal in solution, further evaporation will result in an increase in the concentration of the ion present in greater relative concentration in solution and a decrease in the concentration of the ion present in lower relative concentration (Eugster 1980; Hardie and Eugster 1970).

During the isothermal evaporation experiment, the first salt assemblage was defined by densities ranging from 1.18 to 1.27 g/mL (Fig. 5a). During this period, the concentration of Na^+ dramatically decreased due to the precipitation of halite accompanied with the effect of the principal of chemical divide where the concentration of Cl^- was initially greater than of Na^+. Contrastingly, Mg^{2+} and SO_4^{2-} steadily increased with evaporation until the SO_4^{2-} reached its maximum concentration at a brine density of 1.27 g/mL. The second salt assemblage occurred at brine densities from 1.29 to 1.32 g/mL when K^+ reached its maximum concentration. The SO_4^{2-} concentration began to decline during the second and third salt assemblage, while the Mg^{2+} concentration continued to increase. This is possibly attributable to the precipitation of $MgSO_4$ salts. The third salt assemblage occurred when the brine density was 1.33 g/mL. At this point, the K^+ concentration after reached its maximum value at a density of 1.29 g/mL started to decline at the next densities, while the Cl^- and Mg^{2+} concentration continued to increase in solution. This is possibly due to the precipitation of carnallite. The fourth salt assemblage was observed at densities 1.35–1.36 g/mL. In this salt assemblage, perhaps attributable to the precipitation of $MgCl_2$ salts, the concentration of Mg^{2+} and Cl^- slightly decreased.

Regarding the solar evaporation ponds, the first, second and third salt assemblages appeared at densities of 1.24–1.25, 1.26–1.31 and 1.33 g/mL, respectively (Fig. 5b). The general major ion trends for the three salt assemblages were similar to those of the isothermal evaporation experiment. The Na^+ ion concentration decreased due to precipitation of halite from the beginning of evaporation. Mg^{2+}, K^+, Cl^- and SO_4^{2-} steadily increased with evaporation until the SO_4^{2-} and Cl^- ions reached their maximum concentration at a brine density of 1.25 g/mL. At densities of 1.26–1.31 g/mL, the K^+ and Mg^{2+} began to decline due to the precipitation of carnallite and $MgSO_4$ salts. The concentration of Mg^{2+} slightly decreased while Cl^- increased at the third salt assemblage. This trend is possibly due to the precipitation of $MgCl_2$ salts which would correspond to the fourth salt assemblage observed for the solar evaporation experiment.

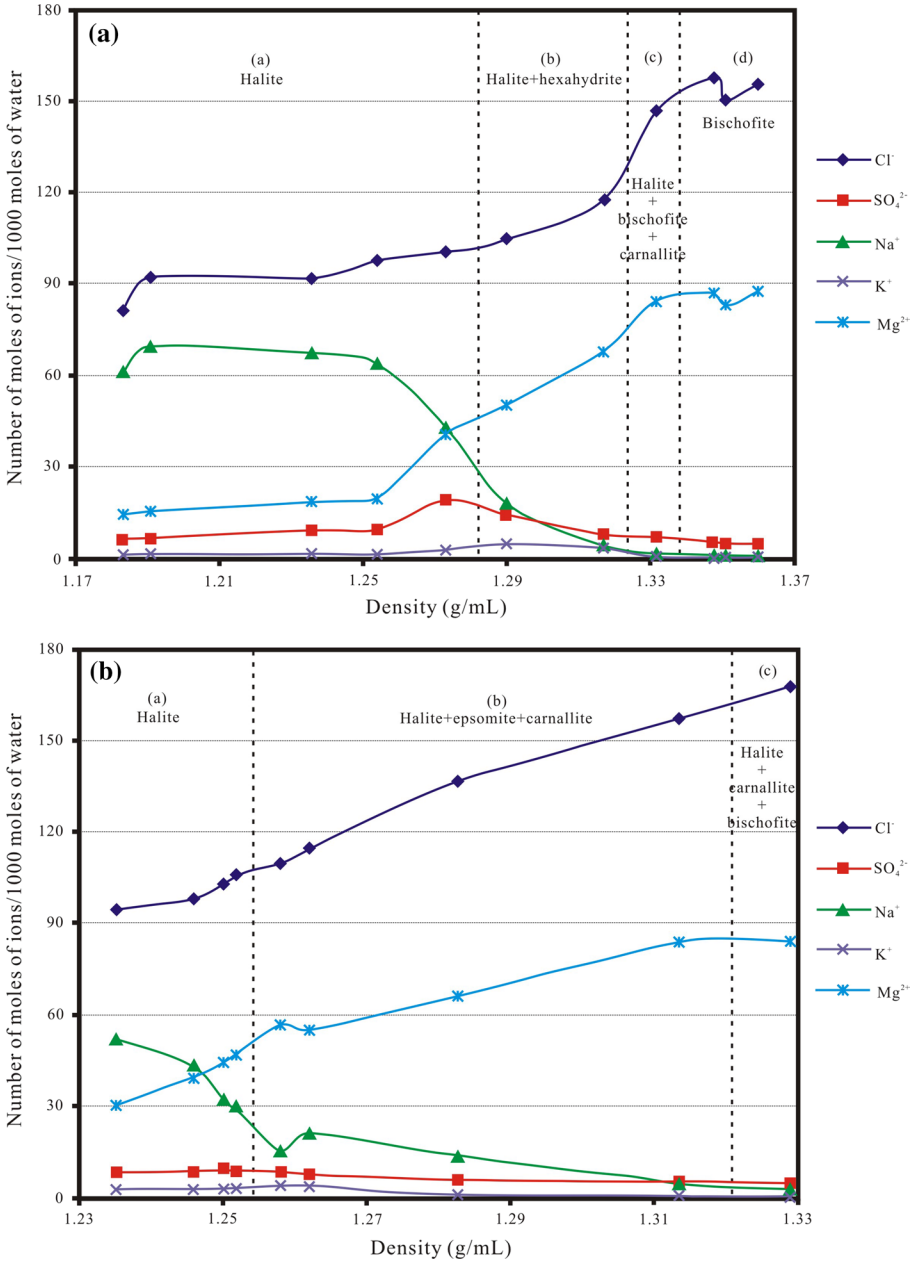

Fig. 5 Evolution of major ion concentrations during **a** isothermal evaporation experiment and **b** solar evaporation ponds. The lower case letters in parentheses are the different salt assemblages. Concentrations of Ca^{2+} and HCO_3^- were too low for display on this graph

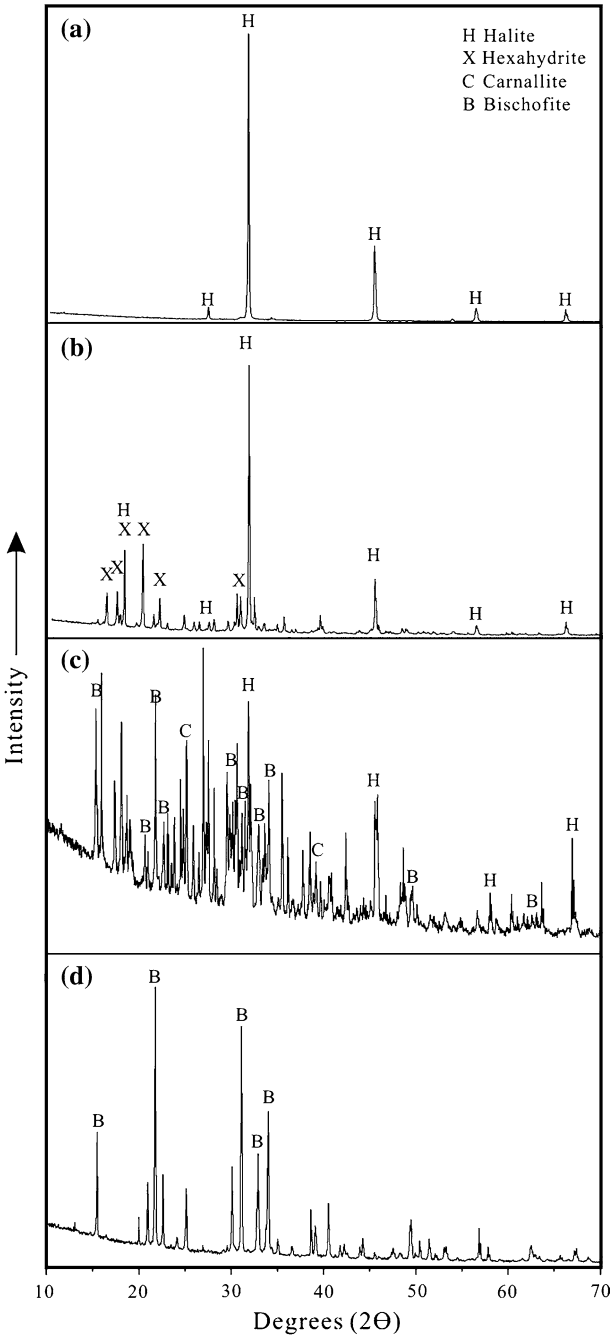

Fig. 6 XRD pattern of salts precipitated throughout the salt assemblage of crystallization at different densities during the isothermal evaporation experiment. The lower case letters in parentheses are the different salt assemblages

3.4 XRD Patterns of the Precipitated Salts

During the isothermal evaporation experiment, the first salt assemblage at densities of 1.24–1.27 g/mL was mainly composed of halite as determined by XRD (Fig. 6a). This finding is in good agreement with the previous results of major ions evolution (see Fig. 5a), where the removal of Na^+ ions from the solution was attributed to NaCl precipitation. The second salt assemblage (1.29–1.32 g/mL) contained hexahydrite and halite (Fig. 6b). The precipitation of hexahydrite was corroborated by the decrease in SO_4^{2-} in the brines (Fig. 5a). The third salt assemblage (1.33 g/mL) precipitated bischofite, carnallite and halite (Fig. 6c). These results agree well with the previous results of major ions evolution during evaporation (see Fig. 5a), where the removal of K^+ ions from the solution was attributed to carnallite precipitation. Bischofite was the only mineral present in the fourth salt assemblage, which precipitated from brines with densities of 1.36–1.35 g/mL (Fig. 6d).

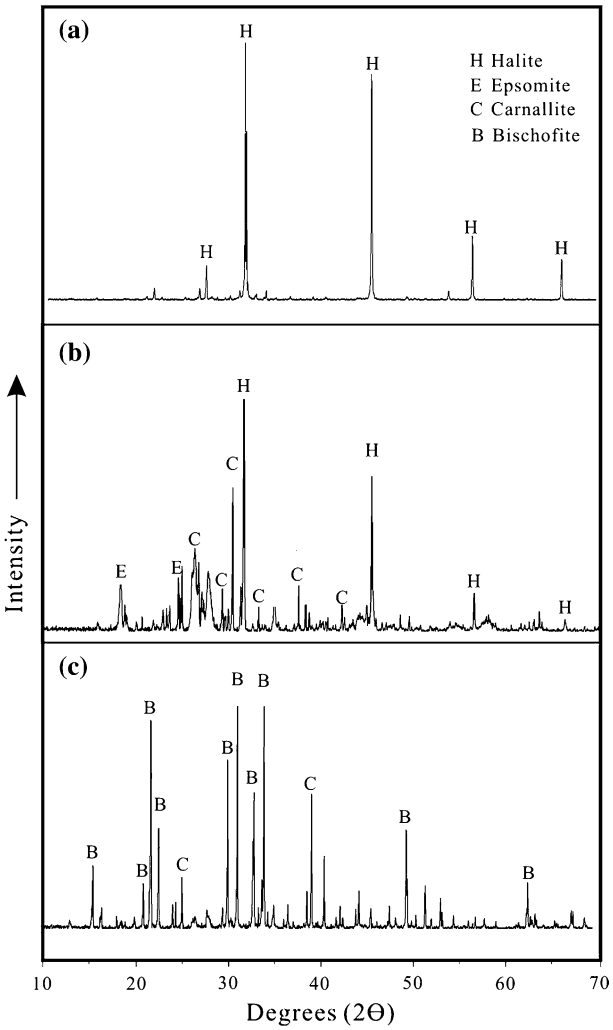

Fig. 7 XRD pattern of salts precipitated throughout the salt assemblage of crystallization at different densities during solar evaporation. The lower case letters in parentheses are the different salt assemblages

The precipitation of bischofite was indicated by the depletion of Mg^{2+} from the solutions during brine evolution (Fig. 5a).

The first salt assemblage that crystallized in the solar evaporation ponds at densities of 1.24–1.25 g/mL was dominated by halite (Fig. 7a), which was similar to the first salt assemblage formed in the isothermal evaporation experiment at similar densities of 1.24–1.27 g/mL. Moreover, these results are consistent with the major ion chemical data where the removal of Na^+ ions from the solution was attributed to NaCl precipitation (see Fig. 5b). Carnallite, epsomite and halite were the main dominant phases that precipitated from brine during the second salt assemblage at densities 1.26–1.31 g/mL (Fig. 7b). The precipitation of epsomite was confirmed by the depletion of SO_4^{2-} from the solutions during evaporation. Furthermore, the results agreed well with major ion chemical data where the removal of K^+ ions from the solution was attributed to carnallite precipitation (see Fig. 5b). The XRD pattern of the third salt assemblage at a density of 1.33 g/mL showed that bischofite formed along with carnallite (Fig. 7c). Again, the precipitation of bischofite was confirmed by the depletion of Mg^{2+} from the solutions during brine evolution (Fig. 5).

3.5 Mineral Assemblage Differences

The crystallization paths of the isothermal evaporation experiment and solar evaporation ponds are expected to follow the salt assemblages: halite → halite + hexahydrite → halite + bischofite + carnallite → bischofite and halite → halite + epsomite + carnallite → halite + carnallite + bischofite, respectively (Table 5). Generally, there was good agreement between the chemical and mineralogical results from both systems, indicating that laboratory conditions sufficiently mimicked those in the field.

However, there were two key differences between the salt assemblages. First, the precipitated magnesium sulfate minerals were different: hexahydrite ($MgSO_4 \cdot 6H_2O$) precipitated

Table 5 The solid phases assembly during the isothermal evaporation and solar evaporation

Solid phases assembly	Sample name	Salt assemblage	Solid phases assembly	Sample name	Salt assemblage
Isothermal evaporation			Solar evaporation		
Halite	GSHZFG12-1	1	Halite	Intake	1
Halite	GSHZFG12-2	1	Halite	Pond 1	1
Halite	GSHZFG12-3	1	Halite	Pond 2	1
Halite + hexahydrite	GSHZFG12-4	2	Halite	Pond 3	1
Halite + hexahydrite	GSHZFG12-5	2	Halite + epsomite + carnallite	Pond 4	2
Halite + bischofite + carnallite	GSHZFG12-6	3	Halite + epsomite + carnallite	Pond 5	2
Bischofite	GSHZFG12-7	4	Halite + epsomite + carnallite	Pond 6	2
Bischofite	GSHZFG12-8	4	Halite + epsomite + carnallite	Pond 7	2
Bischofite	GSHZFG12-9	4	Halite + carnallite + bischofite	Pond 8	3

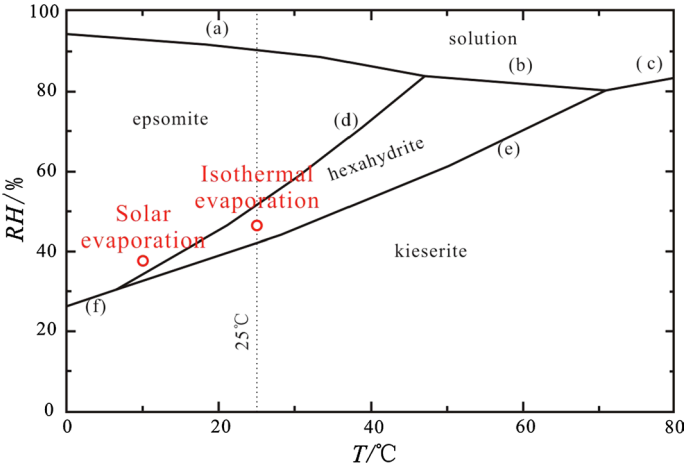

Fig. 8 RH/T phase diagram of $MgSO_4+H_2O$ with deliquescence–crystallization equilibria of **a** epsomite, **b** hexahydrite and **c** kieserite, and hydration–dehydration equilibria of **d** hexahydrite–epsomite, **e** kieserite–hexahydrite and **f** kieserite–epsomite Modified after Steiger and Linnow (2008)

in the experiment, whereas epsomite ($MgSO_4{\cdot}7H_2O$) formed in the solar evaporation ponds. Magnesium sulfate phases are sensitive to temperature and relative humidity (RH), which are likely responsible for this discrepancy (Vaniman et al. 2004). At 25 °C, kieserite and epsomite are the stable phases at RH < 42% and RH > 51%, respectively, with hexahydrate being stable between these relative humidities. Hence, it was expected that the hydration of kieserite starts at RH > 42% with the formation of hexahydrite, while epsomite should be the hydration product at RH > 51% (Fig. 8) (Chou and Seal 2003; Steiger and Linnow 2008). Moreover, the formation temperature of hexahydrite is higher than of epsomite at the same RH. During the isothermal evaporation experiment, the RH and temperature in the laboratory were adjusted to 45% and 25 ± 0.1 °C, respectively. During sampling at the solar evaporation ponds, the RH was 37% and temperature was 10 °C. Based on these environmental conditions, it is expected that hexahydrate and epsomite would be stable magnesium sulfate minerals formed in the isothermal evaporation experiment and solar evaporation ponds, respectively.

In surficial environments, magnesium sulfates, including epsomite and hexahydrite, are commonly associated with the weathering of various metal sulfide deposits, coal deposits and pyritic shales (Jambor et al. 2000). Furthermore, magnesium sulfates are important constituents of evaporative soil environments in cold climates (Keller et al. 1986a, b; Skarie et al. 1987) and of cold desert environments (Keys and Williams 1981). At 37 °C, epsomite is the stable magnesium sulfate in equilibrium with an aqueous solution. The formation of epsomite should be expected based on thermodynamic equilibrium, whereas hexahydrite precipitation is kinetically favored (Skarie et al. 1987). There is also a kinetic hindrance of epsomite formation by hydration of hexahydrite, which is expected at RH > 51%, but is only observed at 80% RH (Vaniman et al. 2004). It is important to note that the concentration of a solution saturated with kieserite contains 9 mol of water per mol of $MgSO_4$. Hence, a large fraction of the liquid water that is formed upon deliquescence is rapidly consumed again if the more hydrated phases such as hexahydrite or epsomite crystallize from the solution. Provided that the precipitation of the hydrated minerals proceeds at a reasonable rate, it could be easily understood that the deliquescence of kieserite could not lead to

bulk solutions filling the pores but rather to solution films that occur during the hydration (Steiger and Linnow 2008). As such, epsomite transforms readily to hexahydrite by the loss of extra-polyhedral water. This transition is reversible and occurs at ≈ 50–55% RH at 298 K and at lower temperatures as the activity of water diminishes (Chou and Seal 2003; Vaniman et al. 2004).

The second mineralogical difference between the precipitates of the experiment and solar evaporation ponds was that the last salt assemblages were bischofite and halite + carnallite + bischofite, respectively. Hence, the salt assemblages formed during late period evaporation are very different. During the evaporation of natural brine from the Salt Lake of central Anatolia, Turkey (Kilic and Kilic 2006), Sebkha el Melah of Zarzis Tunisian (Fezei et al. 2009, 2012), Mg^{2+} and Cl^{-} exhibit conservative behavior until the final precipitation of chloride minerals (e.g., carnallite and bischofite). Moreover, the appearance of bischofite occurs when a brine has reached the late stages of evaporation. In our study, there was a substantial formation of bischofite in the late stage of the isothermal evaporation experiment, indicating that the evaporation intensity was stronger than in the solar evaporation ponds.

3.6 Application for Potassium Deposit Formation

Evaporation of a variety of river and spring water mixtures can produce the saline lake brines that are found at Qarhan Salt Lake (Lowenstein et al. 1989). River waters with SO_4 and HCO_3 in excess of Ca will evolve into calcium-depleted Na–HCO_3–SO_4 brines upon precipitation of calcite. Spring waters, with Ca equivalents greater than SO_4 and HCO_3, evolve into CaCl brines, effectively free of SO_4 and HCO_3. Upon mixing, the chemical divide separating waters that evolve into CaCl brines is approximately 40 parts river water to 1 part spring water. Mixtures between about 40 and 83 parts river water to 1 part spring water produce Na–Cl–SO_4-bearing brines after precipitation of calcite and gypsum; Na–HCO_3–SO_4 brines form from mixtures with a ratio greater than 83:1. Qarhan Salt Lake brines lie along predicted evaporation paths for mixtures of river and spring waters. Thus, brines formed from mixtures with a relatively large proportion of spring inflow evolve into CaCl brines.

A previous study demonstrated that there is deep water recharge into GSL (Ye et al. 2015); however, both the isothermal evaporation experiment and solar evaporation ponds resulted in precipitation of $MgSO_4$ salts, such as hexahydrite and epsomite. Consequently, the ratio of river to spring inflow of brine in GSL is different from Qarhan Salt Lake. Therefore, there are two reasons for the formation of "usual" or $MgSO_4$-bearing potassium deposits. Firstly, there is no deep CaCl spring inflow, and secondly, there is deep CaCl spring inflow recharge, but it is less than 2.5% of the spring inflow. Moreover, during evaporation and salt evolution, the different ratios between river water and CaCl spring inflow could not only form the $MgSO_4$-deficient potassium evaporation mineral sequence, such as Qarhan Salt Lake, but also result in a normal seawater potassium evaporation mineral sequence, such as the Dalangtan Playa (Kong et al. 2014; Wang et al. 2016). Consequently, if the geological structure as well as the hydrogeological and climatic conditions of an inland continental basin is appropriate, nonmarine water may form various potassium evaporite deposits. Thus, we propose that more than half of 50 well-known Phanerozoic $MgSO_4$-deficient marine potash-bearing evaporites in the world (Lowenstein et al. 1989) have been attributed either to nonmarine CaCl spring inflow doping at some time or to

supply of the deep CaCl spring inflow from marine environment. The high concentration of CaCl spring inflow changes the chemical composition of the parent waters from seawater.

4 Conclusions

In both isothermal and solar evaporation of GSL, brine pH decreased while its density increased while various salts precipitated. Both evaporation paths overlapped on the Qinghai Lake water predicted using the Jänecke phase diagram at 25 °C involving the system Na^+, K^+, Mg^{2+}‖Cl^-, SO_4^{2-}–H_2O. Major ion evolutions and mineralogical results showed that the precipitated salts of the isothermal evaporation experiment were halite, epsomite, carnallite and bischofite through four sequential salt assemblages. Alternately, the solid phases forming in the solar evaporation ponds were halite, carnallite and bischofite through three sequential salt assemblages. As a result of differing relative humidity and temperature in the JPFF field and laboratory, hexahydrite and epsomite formed in the isothermal evaporation and solar evaporation, respectively. Moreover, a large amount of bischofite formed in the late stage of the isothermal evaporation experiment, demonstrating that the evaporation intensity was greater than in the solar evaporation ponds.

Although deep CaCl spring inflow recharges the GSL, there was considerable $MgSO_4$ salt formed in both the field and laboratory systems. Moreover, the salt assemblages formed during brine evaporation in GSL belong to $MgSO_4$-bearing group which is similar to those evaporated from the normal seawater. Therefore, two water types could form the "usual" or $MgSO_4$-bearing potassium deposits. The first type water has no deep CaCl spring inflow, while the second type water is a mixture of river to deep CaCl spring inflow (> 40:1). Consequently, different ratios of river and deep CaCl spring waters could not only form the $MgSO_4$-deficient potassium evaporites, but also form normal seawater potassium evaporites. Thus, this study has demonstrated that evaporation of nonmarine waters in continental basins may lead to the formation of potassium deposits with variable mineral assemblages.

Acknowledgements We are grateful to Prof. Z. M. Wang, vice Prof. W. L. Hao, J. Han and X. B. Lin from the Beijing Research Institute of Uranium Geology and vice Prof. J. X. Xu, Doctor T. W. Li, Doctor X. L. Yuan, and Doctor W. L. Miao from the Institute of Salt Lakes, Chinese Academy of Sciences, for their assistance in the field sampling. This research was supported jointly by the National Natural Science Foundation of China (Grant Nos. 41603048, 41473061 and U1407207) and China Geological Survey (Grant Nos. DD20160025 and DD20160054). The manuscript benefited from the insightful review from an anonymous reviewer.

References

Abdel Wahed MSM, Mohamed EA, El-Sayed MI, M'Nif A, Sillanpää M (2015) Crystallization sequence during evaporation of a high concentrated brine involving the system Na–K–Mg–Cl–SO_4–H_2O. Desalination 355:11–21. https://doi.org/10.1016/j.desal.2014.10.015

Casas E, Lowenstei TK, Spencer RJ, Zhang PX (1992) Carnallite mineralization in the nonmarine, Qaidam Basin, China: evidence for the early diagenetic origin of potash evaporites. SEPM J Sediment Res. https://doi.org/10.1306/d4267a05-2b26-11d7-8648000102c1865d

Chen KZ, Bowler JM (1986) Late pleistocene evolution of salt lakes in the Qaidam basin, Qinghai province, China. Palaeogeogr Palaeoclimatol 56:87–104

Chou IM, Seal RR (2003) Determination of epsomite-hexahydrite equilibria by the humidity-buffer technique at 0.1 MPa with implications for phase equilibria in the system MgSO4-H2O. Astrobiology 3:619–630. https://doi.org/10.1089/153110703322610708

Eastoe CJ, Peryt TM, Petrychenko OY, Geisler-Cussey D (2007) Stable chlorine isotopes in Phanerozoic evaporites. Appl Geochem 22:575–588. https://doi.org/10.1016/j.apgeochem.2006.12.012

Eugster HP (1980) Geochemistry of evaporitic lacustrine deposits. Annu Rev Earth Planet Sci 8:35–63

Eugster HP, Harvie CE, Weare JH (1980) Mineral equilibria in a six-component seawater system, Na–K–Mg–Ca–SO_4–Cl–H_2O, at 25°C. Geochim Cosmochim Acta 44:1335–1347

Fan Q, Ma Y, Cheng H, Wei H, Yuan Q, Qin Z, Shan F (2015) Boron occurrence in halite and boron isotope geochemistry of halite in the Qarhan Salt Lake, western China. Sediment Geol 322:34–42. https://doi.org/10.1016/j.sedgeo.2015.03.012

Fezei R, Hammi H, M'nif A (2009) Selective recovery of bischofite from Sebkha El Melah natural brine. Lat Am Appl Res 39:375–380

Fezei R, Hammi H, M'Nif A (2012) Extractive process for preparing high purity magnesium chloride hexahydrate. Chem Ind Chem Eng Q 18:83–88. https://doi.org/10.2298/Ciceq110815049f

Gao F, Zheng M, Song P, Bu L, Wang Y (2012) The 273.15-K-isothermal evaporation experiment of lithium brine from the Zhabei Salt Lake, Tibet, and its geochemical significance. Aquat Geochem 18:343–356. https://doi.org/10.1007/s10498-012-9168-1

Hardie LA (1990) The roles of rifting and hydrothermal $CaCl_2$ brines in the origin of potash evaporites: an hypothesis. Am J Sci 290:43–106

Hardie LA, Eugster HP (1970) The evolution of closed-basin brines. Mineral Soc Am Spec 3:273–290

(JCPDS) JCoPDS (1980) Powder diffraction file search manual, inorganic phases 1980. International Centre for Diffraction Data, Swartmore

Jambor JL, Nordstrom DK, Alpers CN (2000) Metal-sulfate salts from sulfide mineral oxidation. Rev Mineral Geochem 40:302–350

Jensen GKS, Rostron BJ, Duke MJM, Holmden C (2006) Bromine and stable isotopic profiles of formation waters from potash mine-shafts, Saskatchewan, Canada. J Geochem Explor 89:170–173. https://doi.org/10.1016/j.gexplo.2005.11.071

Keller LP, Mccarthy GJ, Richardson JL (1986a) Laboratory modeling of northern great plains salt efflorescence mineralogy. Soil Sci Soc Am J 50:1363–1367

Keller LP, Mccarthy GJ, Richardson JL (1986b) Mineralogy and stability of soil evaporites in North Dakota. Soil Sci Soc Am J 50:1069–1071

Keys JR, Williams K (1981) Origin of crystalline, cold desert salts in the McMurdo region, Antarctica. Geochim Cosmochim Acta 45:2299–2309

Kilic O, Kilic AM (2006) Recovery of salt co-products during the salt production from brine. Desalination 186:11–19. https://doi.org/10.1016/j.desal.2005.05.014

Kong WG, Zheng MP, Kong FJ, Chen WX (2014) Sulfate-bearing deposits at Dalangtan Playa and their implication for the formation and preservation of martian salts. Am Mineral 99:283–290. https://doi.org/10.2138/am.2014.4594

Lowenstein TK, Risacher F (2008) Closed basin brine evolution and the influence of Ca–Cl inflow waters: death Valley and Bristol Dry Lake California, Qaidam Basin, China, and Salar de Atacama, Chile. Aquat Geochem 15:71–94. https://doi.org/10.1007/s10498-008-9046-z

Lowenstein TK, Spencer RJ, Zhang PX (1989) Origin of ancient potash evaporites clues from the modem nonmarine Qaidam Basin of western China. Science 245:1090–1092

McCaffrey MA, Lazar B, Holland HD (1987) The evaporation path of seawater and the coprecipitation of Br^- and K^+ with halite. J Sediment Petrol 57:928–937

Pedley A, Neubert J, van der Klauw S (2016) Potash deposits in Africa introduction, potash deposits of the Republic of Congo, and other African potash deposits and occurrences. Episodes 39:447–457. https://doi.org/10.18814/epiugs/2016/v39i2/95787

Skarie RL, Richardson JL, Mccarthy GJ, Maianu A (1987) Evaporite mineralogy and groundwater chemistry associated with saline soils in eastern North Dakota. Soil Sci Soc Am J 51:1372–1377

Spencer RJ, Lowenstein TK, Casas E, Zhang PX (1990) Origin of potash salts and brines in the Qaidam Basin, China. Fluid Mineral Interact 2:395–408 **(a tribute to Hans Eugster The Geochemical Society Special Publications)**

Steiger M, Linnow K (2008) Hydration of $MgSO_4 \cdot H_2O$ and generation of stress in porous materials. Cryst Growth Des 8:336–343

Sun D, Li B, Ma Y, Liu Q (2002) An investigation on evaporating experiments for Qinghai lake water, China. J Salt Lake Res 10:1–12

Tait AW, Wilson SA, Tomkins AG, Gagen EJ, Fallon SJ, Southam G (2017) Evaluation of meteorites as habitats for terrestrial microorganisms: results from the Nullarbor Plain, Australia, a Mars analogue site. Geochim Cosmochim Acta 215:1–16. https://doi.org/10.1016/j.gca.2017.07.025

Timofeeff MN, Lowenstein TK, da Silva MA, Harris NB (2006) Secular variation in the major-ion chemistry of seawater: evidence from fluid inclusions in Cretaceous halites. Geochim Cosmochim Acta 70:1977–1994. https://doi.org/10.1016/j.gca.2006.01.020

Vaniman DT, Bish DL, Chipera SJ, Fialips CI, Carey JW, Feldman WC (2004) Magnesium sulphate salts and the history of water on Mars. Nature 431:663–665

Wang J, Fang X, Appel E, Zhang W (2013) Magnetostratigraphic and radiometric constraints on salt formation in the Qaidam Basin, NE Tibetan Plateau. Quatern Sci Rev 78:53–64. https://doi.org/10.1016/j.quascirev.2013.07.017

Wang L, Liu C, Gao X, Zhang H (2014a) Provenance and paleogeography of the Late Cretaceous Mengyejing Formation, Simao Basin, southeastern Tibetan Plateau: whole-rock geochemistry, U–Pb geochronology, and Hf isotopic constraints. Sediment Geol 304:44–58. https://doi.org/10.1016/j.sedgeo.2014.02.003

Wang X, Miller JD, Cheng F, Cheng H (2014b) Potash flotation practice for carnallite resources in the Qinghai Province, PRC. Miner Eng 66–68:33–39. https://doi.org/10.1016/j.mineng.2014.04.012

Wang A, Jolliff BL, Liu Y, Connor K (2016) Setting constraints on the nature and origin of the two major hydrous sulfates on Mars: monohydrated and polyhydrated sulfates. J Geophys Res Planets 121:678–694. https://doi.org/10.1002/2015je004889

Warren JK (2016) Evaporites a geological compendium, 2nd edn. Springer, Berlin. https://doi.org/10.1007/978-3-319-13512-0

Ye C, Zheng M, Wang Z, Hao W, Wang J, Lin X, Han J (2015) Hydrochemical characteristics and sources of brines in the Gasikule salt lake, Northwest Qaidam Basin, China. Geochem J 49:481–494. https://doi.org/10.2343/geochemj.2.0372

Zayani L, Rokbani R, Trabelsi-Ayadi M (1999) Study of the evaporation of a brine involving the system Na^+, Mg^{2+}, K^+, Cl^-, SO_4^{2-}–H_2O crystallisation of oceanic salts. J Therm Anal Calorim 57:575–585

Zhang PX (1987) Salt lakes in the Qaidam Basin. Publishing House of Science, Beijing

Zhang PX, Zhang BZ, Lowenstein TK, Pancer RJ (1993) Origin of ancient potash evaporites: examples from the formation of potash of Qarhan Salt Lake in Qaidam Basin. Science Press, Beijing

Zhang X et al (2015) Late Cretaceous potash evaporites in Savannakhet Basin of middle Laos: geochemical evidences of non-marine inputs. Acta Pet Sin 31:2783–2793

Zhang X, Meng F, Li W, Tang Q, Ni P (2016) Reconstruction of Late Cretaceous coastal paleotemperature from halite deposits of the Late Cretaceous Nongbok Formation (Khorat Plateau, Laos). Palaeoworld 25:425–430. https://doi.org/10.1016/j.palwor.2015.11.004

Zhang H, Lu F, Mischke S, Fan M, Zhang F, Liu C (2017) Halite fluid inclusions and the late Aptian sea surface temperatures of the Congo Basin, northern South Atlantic Ocean. Cretac Res 71:85–95. https://doi.org/10.1016/j.cretres.2016.11.008

Zheng M (2011) Resources and eco-environmental protection of salt lakes in China. Environ Earth Sci 64:1537–1546. https://doi.org/10.1007/s12665-010-0601-8

Zheng MP, Liu XF (2009) Hydrochemistry of salt lakes of the Qinghai-Tibet Plateau, China. Aquat Geochem 15:293–320. https://doi.org/10.1007/s10498-008-9055-y

Affiliations

Chuanyong Ye[1] · Jianye Mao[2] · Yaqiong Ren[1] · Yingping Li[3] · Yongjie Lin[4] · Ian M. Power[5] · Yangbing Luo[1]

Chuanyong Ye
yechuanyong@cags.ac.cn

Jianye Mao
327957383@qq.com

Yaqiong Ren
ryaqiong@cags.ac.cn

Yingping Li
liyingping_0820@163.com

Yongjie Lin
linyongjie2014@163.com

Ian M. Power
ianpower@trentu.ca

1 MLR Key Laboratory of Saline Lake Resources and Environments, Institute of Mineral Resources, CAGS, Beijing 100037, China

2 Qinghai Geological Survey Institute, Xining 810012, Qinghai, China

3 Jinzhong Vocational and Technical College, Yuci 030600, Shanxi, China

4 School of Earth Sciences and Resources, China University of Geosciences, Beijing 100083, China

5 Trent School of the Environment, Trent University, 1600 West Bank Drive, Peterborough, ON K9L 0G2, Canada